ELSEVIER

Ultramicroscopy 72 (1998) 199–211

ultramicroscopy

The determination of rigid lattice shifts across delta-doped layers using regressional analysis

R.E. Dunin-Borkowski*,[1], W. Michael Stobbs[2]

Department of Materials Science and Metallurgy, University of Cambridge, Cambridge CB2 3QZ, UK

Received 4 November 1996; received in revised form 9 December 1997

Abstract

We present a simplified approach for determining the rigid lattice shift across an interlayer from a high-resolution lattice image. The approach is illustrated through the analysis of delta-doped layers in Si and GaAs, for which the lattice shifts are measured to accuracies of better than ± 7 pm. The results are compared with the predictions of continuum elasticity theory, and some surprising discrepancies are noted. In particular, for Si delta-doping in GaAs the measured lattice contractions do not follow the predicted linear increase with dopant concentration and are much larger than the theory would predict. © 1998 Elsevier Science B.V. All rights reserved.

Keywords: Regressional analysis; Rigid lattice contraction; Delta-doping; HREM

1. Introduction

Wood et al. [1] demonstrated that the rigid lattice shift across a narrow interlayer can be determined from a high-resolution image by analyzing the misregistry between lattice fringes that have been extrapolated from regions of identical thickness, defocus and orientation on each side of the layer. They also showed that the reliability of the results can be assessed by plotting the measured lattice shift as a function of both the widths of the regions analyzed and their distances from the layer. This ensures that the effects of diffraction and phase contrast at the layer are discounted. If the imaging conditions are unchanged between the two regions of the image analyzed, then the accuracy achieved can approach 1% of the lattice fringe spacing [2].

Our aim here is to present a simplified method of applying this "regressional analysis" technique. We illustrate our approach by determining the lattice shifts across delta-doped layers in Si and GaAs. These comprise sheets of ionized dopant atoms that are nominally confined to substitutional sites in one atomic layer of the host lattice [3]. Our experimental measurements will be compared with the predictions of continuum elasticity theory, as well as with contributions to the lattice shifts from the electric fields that are expected to be present at such layers. The results are primarily of interest to us for

* Corresponding author.

[1] Present address: Center for Solid State Science, Arizona State University, Tempe, AZ 85287-1704, USA.

[2] Deceased 26.4.1996.

0304-3991/98/$19.00 © 1998 Elsevier Science B.V. All rights reserved.
PII S0304-3991(98)00003-5

interpreting the local forward scattering potential profiles at such layers, which we have measured using Fresnel contrast analysis [4], as this requires a knowledge of the changes in density at the layers. In the present work, we will also use digitally generated moiré fringes (formed by adding perfect reference gratings to the lattice images) both in order to choose regions of maximum lattice fringe contrast for regressional analysis and to confirm that no long-range distortions are present in the images.

The high-resolution images presented here were obtained at 400 kV using a JEOL 4000EXII microscope ($C_S = 0.9$ mm, $C_C = 1.3$ mm) and an objective aperture of semi-angle 20 mrad. Cleaved wedge specimens were examined, primarily so that areas of uniform thickness could be analyzed, and also because amorphous surface layers would then be thinner and because the position of the doped layers could be established from the contrast visible in very thick regions. The effects of knock-on damage were minimized by always aligning the microscope away from the areas of interest.

2. The application of regressional analysis and moiré fringes to delta-doping

2.1. Regressional analysis

We begin by describing the procedure that will be used to determine the lattice shift across each of the delta-doped layers. The approach involves the projection of a region of a high-resolution image containing the doped layer at its center parallel to the lattice fringes in the direction of the layer. Polynomial fits are used to determine the position of each peak and trough in the lattice fringe profile. The mismatch between the lattice fringes extrapolated from regions on each side of the layer is then measured by plotting the fringe position y as a function of fringe number x and using the following simple algorithm:

Referring to the schematic diagrams shown in Fig. 1, if the fringe positions in perfect regions of crystal on either side of the layer are described by the equations

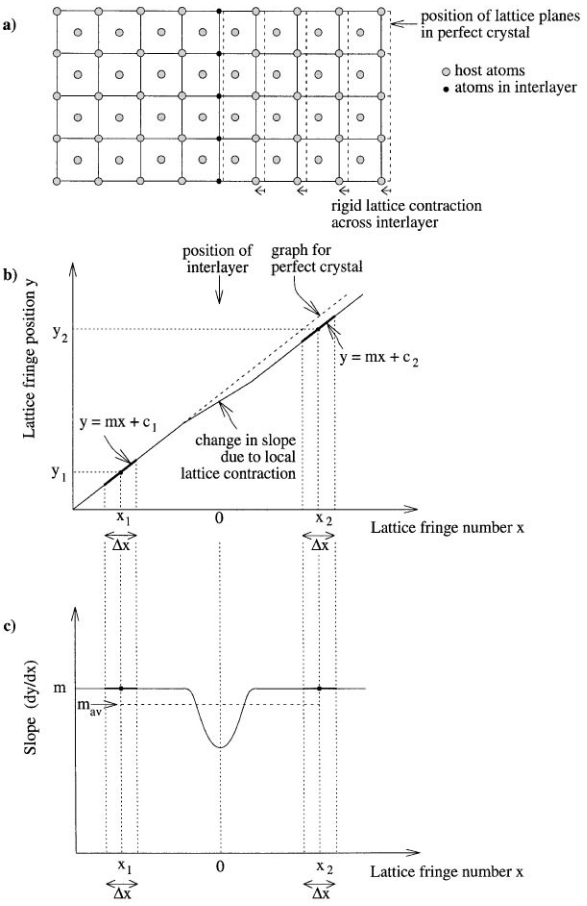

Fig. 1. (a) Schematic diagram showing a rigid lattice contraction across a narrow interlayer. The associated graphs of (b) lattice fringe position y and (c) lattice fringe spacing (dy/dx), plotted as a function of fringe number x, illustrate the symbols used to determine the rigid lattice shift across the layer.

$$y = mx + c_1$$

and

$$y = mx + c_2$$

(the slope m should be the same in the two regions), then the rigid shift of the lattice across the layer d_{rc} is given by $(c_2 - c_1)$, which is negative for a lattice contraction. If the slopes are measured by analyzing regions of width Δx at positions x_1 and x_2 in a graph of fringe spacing (dy/dx) plotted as a function of x, and if the average slope between x_1 and x_2 is

$$m_{av} = \left(\frac{y_2 - y_1}{x_2 - x_1}\right),$$

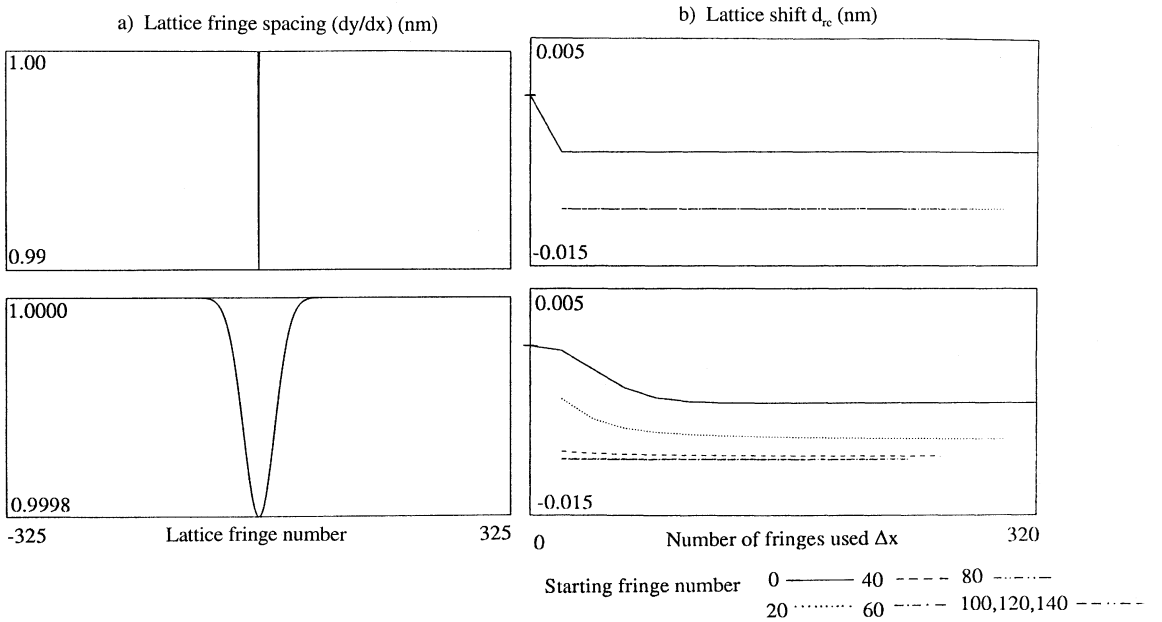

Fig. 2. Simulated graphs of (a) lattice fringe spacing (dy/dx) in nm for a rigid lattice shift of 0.01 nm distributed over different numbers of atomic layers, and (b) corresponding values of the lattice shift d_{rc} in nm that would be inferred using the approach described in the text, plotted as a function of the fringe number from the layer x and the width of the two regions analyzed Δx. (The lower trace in each graph has the calculations for many starting fringe numbers superimposed).

then

$$d_{rc} = (c_2 - c_1) = (x_2 - x_1)(m_{av} - m).$$

Fig. 2a shows simulated plots of lattice fringe spacing (dy/dx) plotted as a function of lattice fringe number, which correspond to identical rigid lattice shifts of 0.01 nm across a narrow layer, but have the strain distributed over different numbers of atomic layers. The values of d_{rc} that would be inferred from these profiles using the present approach are shown in Fig. 2b as a function of both the starting fringe number and the widths of the regions analyzed, and can be seen to provide the correct value of d_{rc} so long as the fringe spacing is no longer varying within the two regions analyzed.

The primary advantage of the present approach is that it is both straightforward and rapid to apply. In contrast to the direct measurement of local lattice fringe displacements in two dimensions [5], it also allows systematic errors in the measured rigid lattice shifts to be assessed and discounted. Such systematic errors may result from the presence of diffraction and phase contrast at the layer, and have been discussed in detail by Wood et al. [1] and Stobbs et al. [2].

2.2. Moiré fringes

In the examples presented below, both the orientation used for projecting the lattice fringes and the thicknesses at which they exhibited maximum contrast were established using moiré fringes formed by digitally superimposing perfect reference gratings (images containing sinusoidal fringes in one direction) onto the experimental images. Moiré fringes were also formed "optically" by double-exposing a sheet of photographic paper first with a reference grating and then with the experimental lattice image [6], in order to discount the possibility of a large or long-range distortion field that would not be interpreted correctly using regressional analysis.

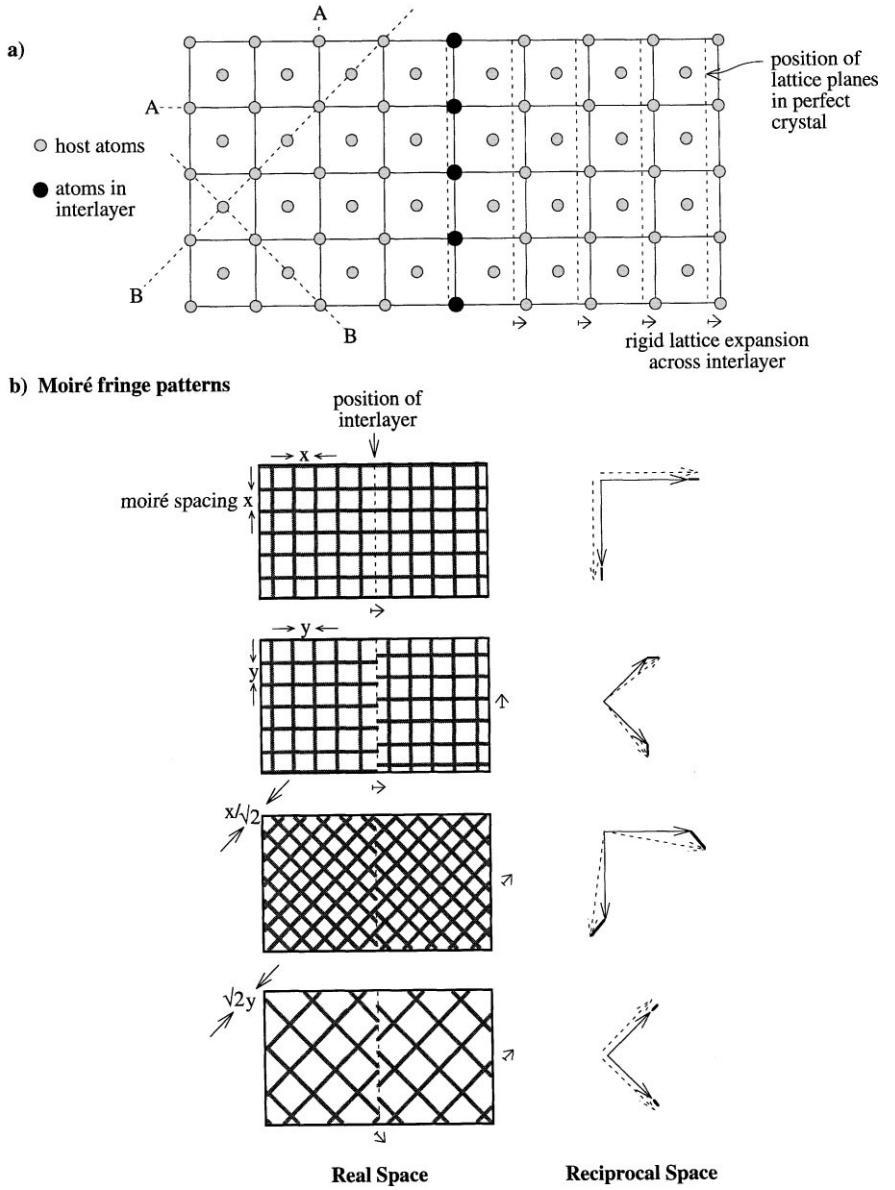

Fig. 3. The effect of (a) a real-space rigid lattice expansion across a narrow interlayer, on (b) the moiré fringes that would be formed using several different sets of experimental and reference fringes which are depicted using both real and reciprocal space constructions and are shown in the left- and right-hand columns, respectively. The first and third pairs of diagrams from the top are formed using 'A' lattice fringes (e.g. 004 for Si); while the second and fourth pairs are formed using 'B' lattice fringes (e.g. 022 for Si).

Fig. 3 summarizes the moiré fringe patterns that might be formed in the presence of a large rigid lattice shift (in this case an expansion) using two different sets of experimental fringes.

3. Experimental results

The specimens examined, whose structures are shown schematically in Fig. 4, were grown on

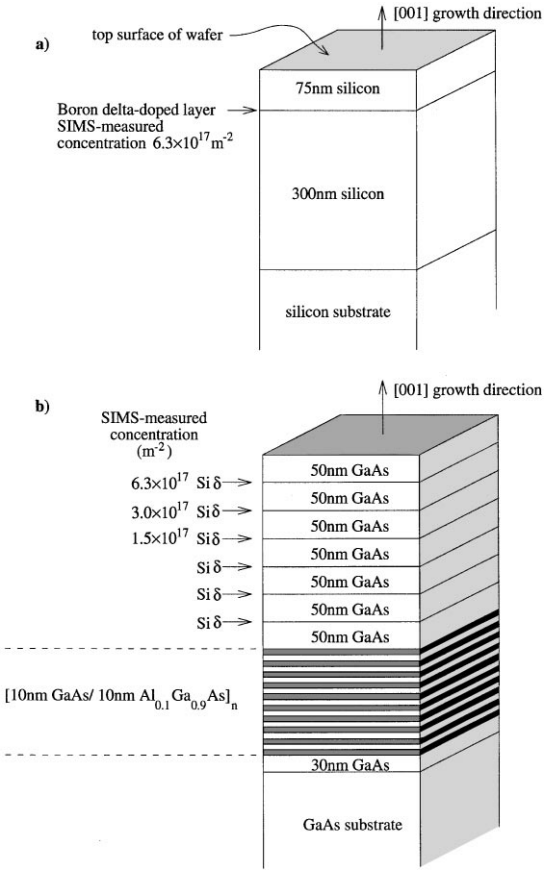

Fig. 4. Schematic diagrams of (a) the B delta-doped layer in Si and (b) the Si delta-doped layers in GaAs examined here.

[0 0 1] substrates using molecular beam epitaxy at temperatures at which the dopants are expected to be fully substitutional. The B delta-doped layer in Si was grown at a temperature of 480°C, secondary ion mass spectrometry (SIMS) data indicating a sheet B concentration (if all of the impurities were confined to one atomic layer) of 24 at%, and X-ray diffraction data indicating a layer width of approximately 0.5 nm. The GaAs specimen contained six Si delta-doped layers of increasing concentration, which were grown 50 nm apart at a temperature of 500°C. Only the three highest concentration layers were analyzed, corresponding to SIMS-measured sheet concentrations of 10.1, 4.8 and 2.4 at%.

3.1. B delta-doping in Si

Fig. 5 shows (at a magnification that is too low for the lattice fringes to be visible) a high-resolution image of a cleaved wedge specimen containing the Si : B layer, taken at the [1 0 0] zone axis at a magnification of 300 k and a measured defocus of 62 nm underfocus, which has been digitized at a resolution of 5.6 pixels/004 fringe. Faint (and defocus-dependent) contrast of width approximately 1.5 nm is visible at the position of the layer. However, this is not expected to affect the lattice fringe spacings far from the layer. As the 004 fringes in the image are not exactly perpendicular to the specimen edge, two regions of the image, which are marked in Fig. 5, were analyzed below – one perpendicular to the 004 fringes and one parallel to contours of constant crystal thickness. The digitally generated moiré fringes in Fig. 6a show immediately which regions of the image exhibit maximum 004 fringe contrast (following contours of constant thickness)[3]. Fig. 6b and Fig. 6c show a typical section of the projected lattice fringes from a small part of region B and their spacings close to the position of the layer. No local variations in fringe spacing are seen in Fig. 6c, suggesting that any lattice shift is small and is at this stage masked by the sampling of the fringes.

Experimentally, care was taken with the data analysis in the following respects. Slow variations in fringe spacing across the image, caused by barrel distortions in the microscope and densitometer lenses [7], were removed by subtracting a linear background from the graph of fringe spacing so that the effect of the higher frequency variations in spacing could be assessed. (Such background variations were often found to reverse in sense when the same image was digitized on successive occasions.) The angle of the 004 fringes was optimized with respect to the densitometer pixel columns during digitization, the sampling of the fringes was then increased by a factor of five by interpolation, and the image was convolved with a Gaussian of width

[3] The 004 fringes in Si disappear periodically with thickness whenever the 022 amplitude, which double diffracts into 004, goes to zero.

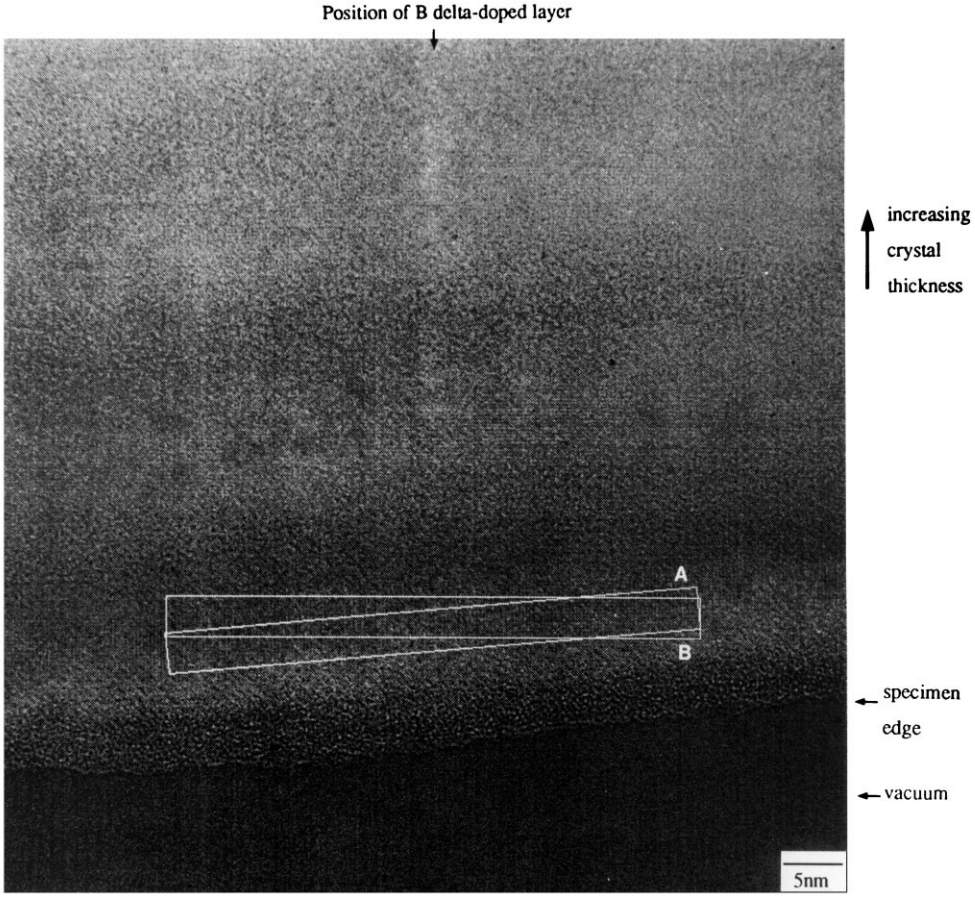

Fig. 5. Lattice image of a cleaved wedge specimen of the Si : B layer at a measured defocus of 62 nm underfocus, showing the regions used for subsequent analysis ((A) constant thickness; (B) perpendicular to the 004 lattice fringes).

approximately one fifth of the 004 fringe spacing before determining the fringe positions.

Fig. 7a shows for region B the rigid lattice shift determined as a function of the number of fringes Δx and the starting fringe number $|x| = (|x_i| - \Delta x/2)_{i=1,2}$, both for all values of $|x|$ and Δx and for values of $|x| > 100$ and $\Delta x > 80$. The similarity to the simulated graphs in Fig. 2 is evident, the plots for large starting fringe numbers providing the more reliable data. The graphs are consistently below the value of zero marked on the vertical axis, which corresponds to an overall contraction of the Si lattice across the B-doped layer, while the magnitudes of the measured shifts generally stay within a small fraction of an 004 fringe spacing (less than about 0.02 nm). This agrees with the lack of a detectable shift in the "optical" moiré fringe pattern shown in Fig. 8. Fig. 7b and Fig. 7c illustrate the effect on the measured lattice shift of smoothing the graph of fringe *spacing* by convolving it once and five times with a Gaussian of width 2.5 times the 004 fringe spacing. The values obtained for the lattice shifts (defined here to be the mid-points of the ranges over which they vary) are summarized in Table 1 and are consistent between the two regions analyzed. The decrease in the values of the measured shifts as the graph of fringe spacing is smoothed may result from the progressively smaller

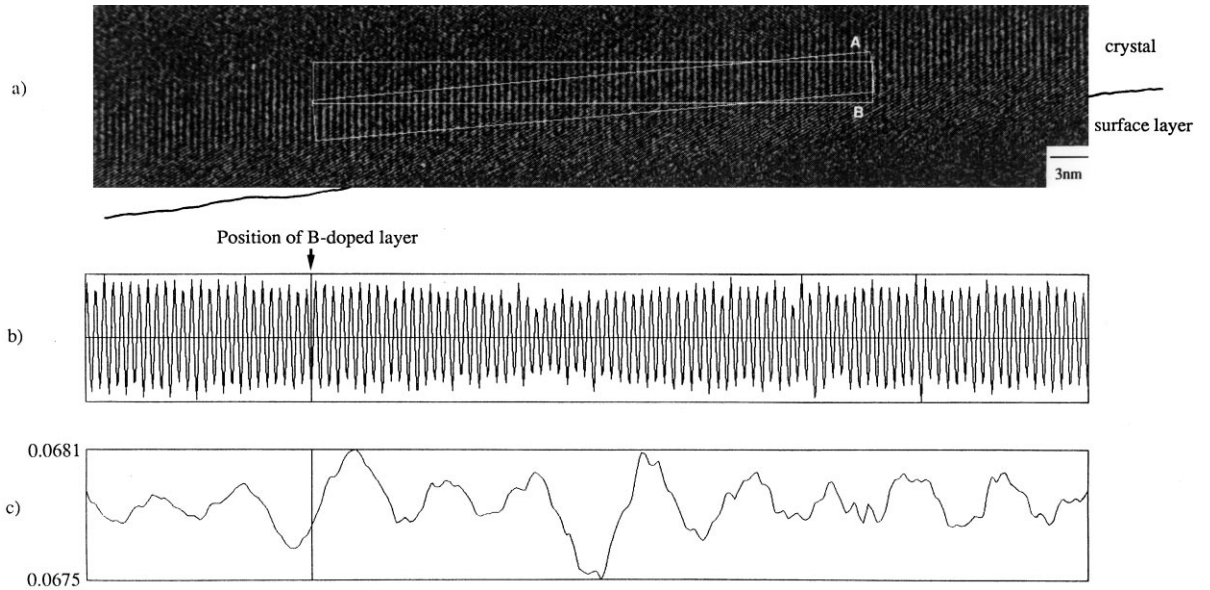

Fig. 6. (a) Digitally generated *moiré* fringe pattern used for establishing regions of maximum 004 fringe contrast for regressional analysis. Region A is at constant crystal thickness and region B is oriented perpendicular to the 004 lattice fringes; (b) Typical section of the projected *lattice* fringes close to the center of the B-doped layer; (c) The corresponding graph of fringe spacing plotted as a function of fringe number.

effect of outlying points in the data[4]. We choose a value for the measured lattice contraction of (12.6 ± 6.1) pm, which is the mid-point of the values in the unsmoothed and smoothed graphs.

3.2. Si delta-doping in GaAs

A lattice image of a cleaved wedge specimen containing the Si delta-doped layers in GaAs, taken at the [1 0 0] zone axis at a nominal magnification of 400 k and a measured defocus of 45 nm underfocus, was digitized at a resolution of 7.4 pixels/004 fringe, with the 004 lattice fringes almost parallel to the densitometer pixel columns. Regions of the image corresponding to the positions of the three highest concentration delta-doped layers were chosen for further analysis by establishing the thickness ranges that exhibited maximum 004 fringe contrast using digitally generated moiré fringe patterns. The lattice shifts were determined for each of the three highest concentration doped layers, as well as for a region of pure GaAs. Fig. 9 shows for the 2.4 at% Si-doped layer the equivalent graphs to those shown for Si : B in Fig. 7. As for Si : B, the graphs for all three doped layers are indicative of a contraction of the GaAs lattice. The magnitudes of the contractions are all below 0.03 nm, which again agrees with the lack of a detectable shift in the "optical" moiré fringes shown superimposed onto the [1 0 0] lattice image in Fig. 10. No change in the measured lattice contractions was observed on smoothing the fringe spacings, and accordingly the results summarized in Table 2 are averages of unsmoothed and smoothed measurements. Reassuringly, the value of the lattice shift measured across pure GaAs is zero to within experimental error, and there

[4] The definition of an error in the experimental measurements is complicated by the fact that the data points are not independent: we choose here to define the error (perhaps pessimistically) as one half of the full spread of the data.

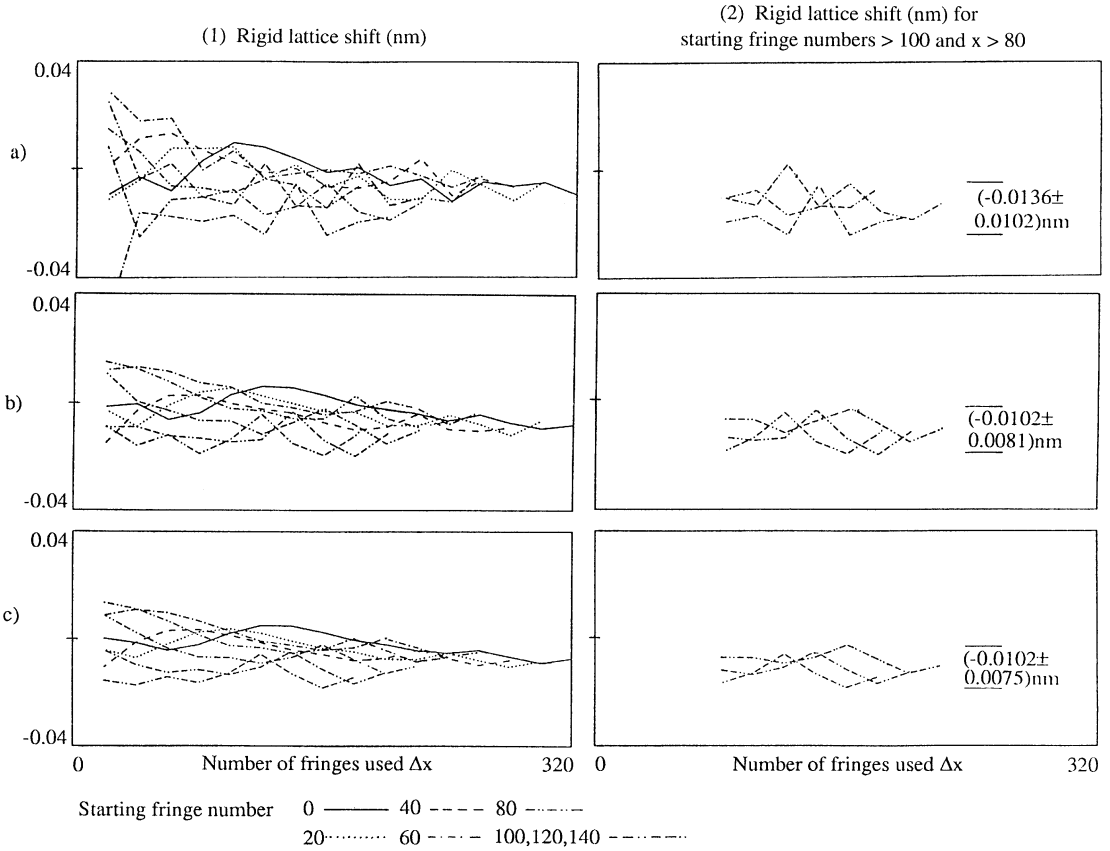

Fig. 7. Calculated rigid lattice shift in nm for region B in Fig. 6, plotted as a function of the number of fringes and the starting fringe position used. Slope smoothed (a) 0, (b) 1 and (c) 5 times (see text). (1) all starting fringe numbers and values of Δx; (2) starting fringe numbers above 100 and Δx values greater than 80.

is a monotonic increase in the observed lattice contraction with Si concentration.

4. Discussion

We now compare the measured lattice contractions with theoretical predictions and with experimental data from other sources. A lattice contraction coefficient β for substitutionally B-doped Si has been determined by Holloway and McCarthy [8] using double-crystal X-ray diffractometry. If a_o is the host (Si) lattice parameter, N_P the dopant concentration (area or volume) in units of at%, and da_o the change in a_o from the value that it takes for $N_P = 0$, then β can be defined[5] according to the relation

$$da_o = \left(\frac{-8\beta}{100a_o^2}\right) N_P$$

and has a measured value of 5.19×10^{-30} m^3. For convenience, we will refer to da_o as $-\gamma N_P$, so that

[5] da_o is more conventionally expressed as being proportional to the dopant concentration *per unit volume* rather than the dopant concentration in units of at%. While the former choice is applicable for dopant concentrations of a few at% or less, it would result in a_o diverging unrealistically with increasing dopant concentration at the larger concentrations of interest here.

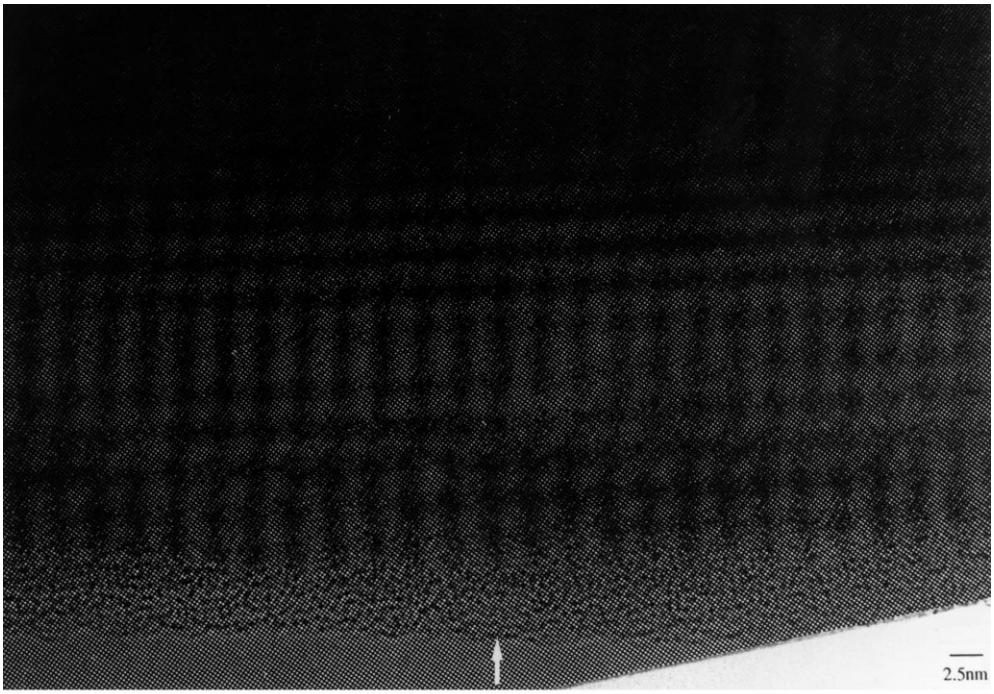

Fig. 8. "Optical" moiré fringes superimposed onto the lattice image of the B delta-doped layer in Si. The position of the layer is marked.

Table 1
Rigid lattice shifts for Si : B, determined using values of $|x| > 100$ and $\Delta x > 80$, from graphs of fringe spacing which have been smoothed by different amounts (see text). The errors quoted are defined as half of the total variation in the measured values

Region analyzed	Measured rigid lattice shift (pm)		
	Unsmoothed	Smoothed 1	Smoothed 5
Perpendicular to 004 fringes	-13.6 ± 5.1	-10.2 ± 4.0	-10.2 ± 3.8
Constant thickness	-13.2 ± 5.3	-10.2 ± 3.4	-9.0 ± 2.4
Average values	-13.4 ± 5.2	-10.2 ± 3.7	-9.6 ± 3.1

the lattice parameter of the bulk doped semiconductor $a' = (a_o - \gamma N_P)$ and $\gamma = 1.41$ pm for B doping in Si. This compares favorably with the value of 1.35 pm which would be predicted from the ionic radii for B and Si given in Table 3 [9,10] using the relation

$$\gamma = \left(\frac{a_o(\mathrm{Si})}{100}\right)\left(1 - \frac{r_B}{r_{Si}}\right).$$

A corresponding lattice contraction coefficient was not available for Si doping in GaAs, and so values of γ were calculated from the ionic radii in Table 3, giving

$$\gamma(\text{amphoteric doping}) = \left(\frac{a_o(\mathrm{GaAs})}{100}\right)\left(1 - \frac{2r_{Si}}{r_{Ga} + r_{As}}\right)$$

$$= 0.232 \text{ pm},$$

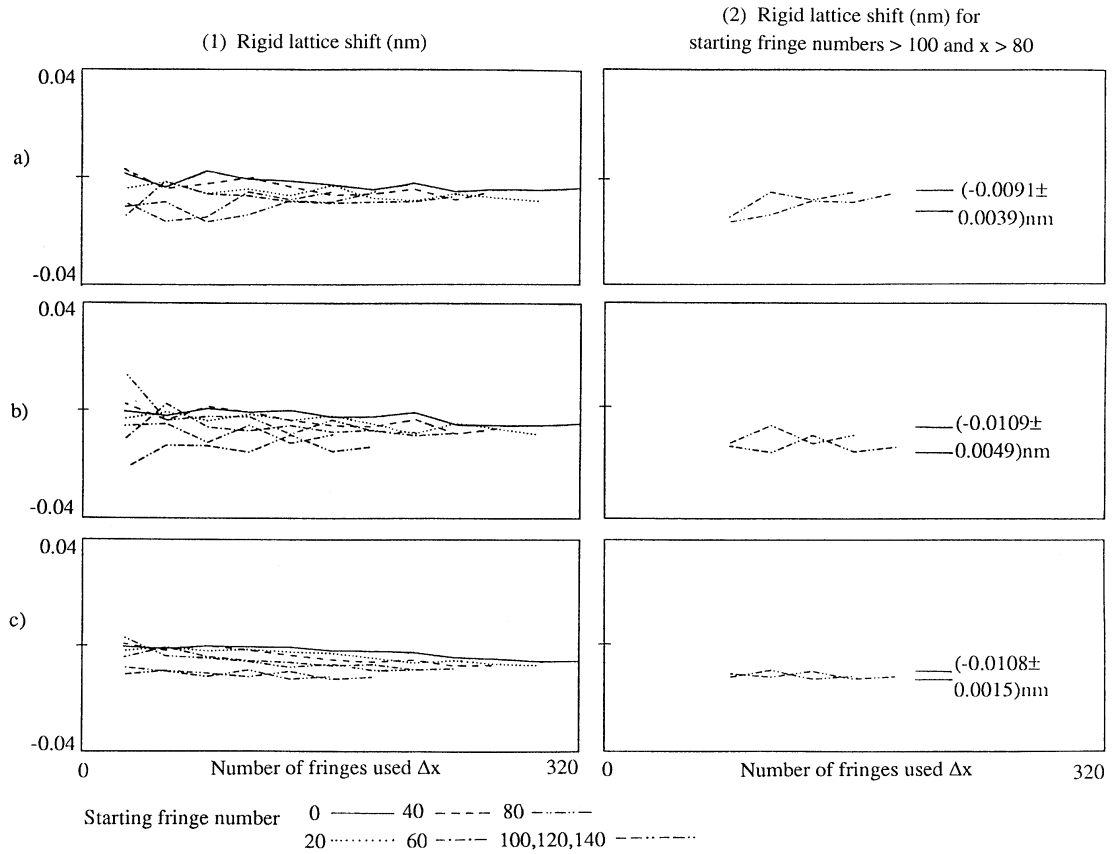

Fig. 9. As for Fig. 7, but for the Si delta-doped layer with a SIMS-measured concentration of 2.4 at%.

$$\gamma(\text{Si on Ga sites only}) = \left(\frac{2a_o(\text{GaAs})}{100}\right)\left(\frac{r_{Ga} - r_{Si}}{r_{Ga} + r_{As}}\right) = 0.417 \text{ pm},$$

$$\gamma(\text{Si on As sites only}) = \left(\frac{2a_o(\text{GaAs})}{100}\right)\left(\frac{r_{As} - r_{Si}}{r_{Ga} + r_{As}}\right) = 0.0463 \text{ pm}.$$

Assuming that a delta-doped layer is constrained to match the host lattice in the plane of the dopant, and has a lattice parameter perpendicular to the plane of the layer given by $a_\perp$, the magnitude of $a_\perp$ takes the form [11]

$$a_\perp = a_o - \left(\frac{1+\upsilon}{1-\upsilon}\right)\gamma N_P,$$

where the Poisson ratio υ takes a value of 0.28 in Si and 0.31 in GaAs [12] and we assume that υ is unaffected by the presence of the dopant. The rigid shift d_{rc} across a doped layer with a total sheet concentration N_P is then

$$d_{rc} = \left(\frac{1}{4}\right)\left(\frac{1+\upsilon}{1-\upsilon}\right)\gamma N_P,$$

and is independent of the number of atomic layers over which the dopant has spread. (The factor of $\frac{1}{4}$ in the expression for d_{rc} is required because N_P now describes the dopant concentration were it all in a single atomic layer of thickness $\frac{1}{4}\,a_o$). The predicted lattice contractions for Si : B and GaAs : Si are plotted in Fig. 11 alongside the experimental results.

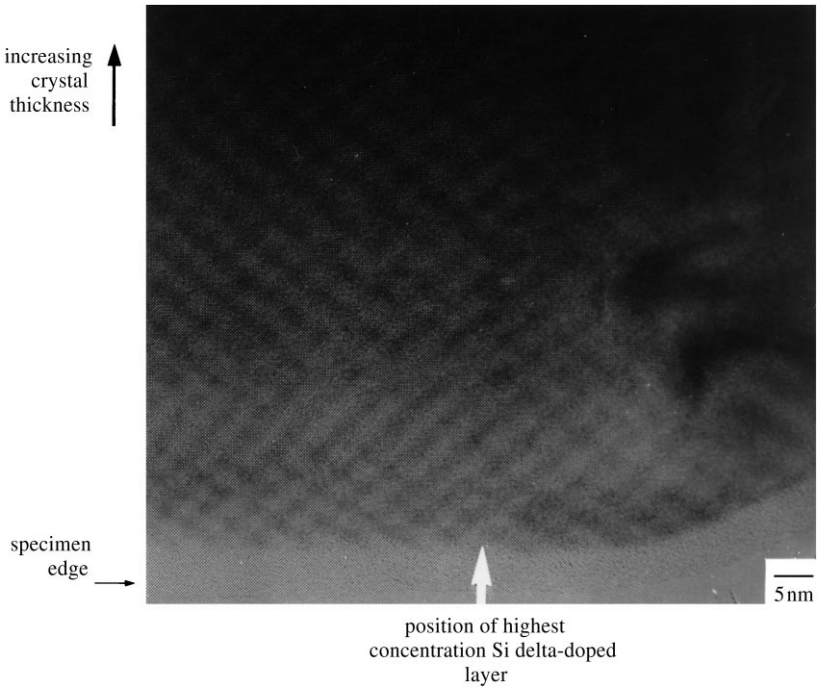

Fig. 10. "Optical" moiré fringes superimposed onto a lattice image of a cleaved wedge specimen at the position of the highest concentration Si delta-doped layer analyzed here.

Table 2
Rigid lattice shifts for GaAs : Si, averaged over the values obtained from unsmoothed and smoothed graphs of lattice fringe spacing (see text)

SIMS-measured concentration (at%)	Measured rigid lattice shift (pm)
10.1	-19.6 ± 2.0
4.8	-13.8 ± 2.2
2.4	-10.3 ± 0.5
0 (pure GaAs)	0.4 ± 1.9

For the Si : B, the measured lattice contraction of (12.6 ± 6.1) pm corresponds to a sheet dopant concentration of (20.1 ± 9.7) at% and the consistency with the SIMS-measured concentration of 24 at% B is reassuring. A lattice contraction of (31 ± 2) pm for 56 at% B delta-doping in Si has been measured by Powell et al. [13] using double-crystal X-ray diffraction, corresponding to a "lattice contraction per at% B" of (0.55 ± 0.04) pm; the value for (12.6 ± 6.1) pm and 24 at% B is (0.53 ± 0.25) pm.

The results for Si delta-doping in GaAs are far more surprising. Whereas the lattice contraction should be proportional to dopant concentration, the experimental data are not only more indicative of an asymptotic relationship, but are also much larger than the predicted values. This anomaly may be associated either with the presence of defects in the form of vacancies or other impurities at the layers [14] or with the great strength of the Si–As bond (if Si were to substitute predominantly for Ga) compared with that of the Ga–As bond. No evidence for cluster formation (inhomogeneity of the dopant) was observed in cross-sectional samples of the same layers, and such a phenomenon could not in any case account for the magnitude (or the sign) of the observed lattice contraction. Confidence in the results obtained here is provided by a lattice contraction of (5.6 ± 1.1) pm in a GaAs : Si

Table 3
Ionic radii, taken from Suchet [9] and Pearson [10]

Element	Ionic radius (nm)
B	0.088
Si	0.117
Ga	0.126
As	0.118

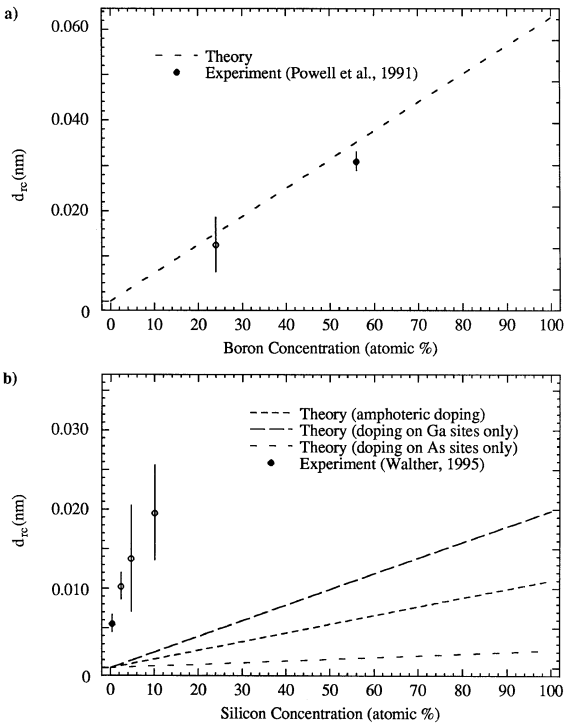

Fig. 11. Calculated values of the magnitude of the lattice *contraction* d_{rc} for (a) B delta-doping in Si and (b) Si delta-doping in GaAs, together with the experimental results from the present work (shown as open circles) plotted as a function of the SIMS-measured dopant concentrations. An experimental X-ray diffraction result from Powell et al. [13] for Si : B and an experimental TEM result from Walther [15] for GaAs : Si are also shown.

delta-doped layer with a sheet dopant concentration of 0.4 at%, measured using a similar approach to that presented here [15], which is also shown in Fig. 11 and is consistent with the present results and not with the predictions. Evidence for the presence of anomalously large lattice contractions in bulk Si-doped GaAs has also been reported by Fewster and Willoughby [16] and Watson et al. [17].

It should be noted that a further contribution to the strain at a delta-doped layer is possible. This arises from the electrostatic attraction of the "bound" dopant ions (the narrower charge distribution) to the "free" charge carriers (the wider charge distribution). Although this contribution should always result in an expansion of the lattice [18] and hence cannot explain the lattice contraction seen for GaAs : Si here, its magnitude should still be considered. For a bound charge distribution of width less than approximately 2 nm, the width of the free charge distribution is given by

$$d_f = 200\sqrt{\frac{7}{5}}\left(\frac{h^2 a_0^2 \varepsilon_0 \varepsilon_r}{18\pi^2 e^2 m^* N_P}\right)^{1/3}$$

where m^* is the free carrier effective mass [3]. Table 4 summarizes calculated values of d_f for 24 at% p-type B delta-doping in Si, 10.4 at% Si n-type delta-doping in GaAs, and 1 at% delta-doping in each material, the lower values representing the possibility of incomplete electrical activity of the dopant. The magnitudes of the corresponding lattice expansions, calculated using the relations presented by Dunin-Borkowski et al. [18], are also given for both Gaussian and exponential limits for the forms of the charge distributions, for a "bound" charge distribution of width $d_b = 0.2$ nm. The values indicate that electrostatic attraction is not a major contribution to an observed rigid lattice shift for the dopant concentrations that have been characterized here, but may become significant for electrically active concentrations greater than 50 at%.

5. Conclusions

The regressional analysis technique has been applied to the determination of the rigid lattice shifts across delta-doped layers in Si and GaAs. The measured lattice contractions are (12.6 ± 6.1) pm for a SIMS-measured sheet concentration of 24 at% for B delta-doping in Si, and (19.6 ± 6.0), (13.8 ± 6.7) and (10.3 ± 1.7) pm for 10.1, 4.8 and

Table 4
Electrostatic contributions to the lattice expansions at delta-doped layers containing "bound" charge distributions with half-widths of 0.2 nm, for charge distributions which are Gaussian and exponential in form (see Ref. [18]). The values of d_f have been calculated using the relations given by Schubert [3]. (ε_r = relative permittivity, assumed to be unaffected by the presence of the dopant, and, Y_{001} = Young's modulus in the [0 0 1] direction)

Material	Sheet dopant concentration (at%)	d_f (nm)	Lattice expansion (pm) for charge of	
			Gaussian form	Exponential form
B delta-doped (p-type) Si	24	0.7	0.073	0.13
$\varepsilon_r = 11.9$,	1	2.1	0.00018	0.00036
$Y_{001} = 1.3 \times 10^{11}$ Nm^{-2}				
Si delta-doped (p-type) GaAs	10.1	2.0	0.021	0.043
$\varepsilon_r = 13.1$,	1	4.3	0.00023	0.00049
$Y_{001} = 8.5 \times 10^{10}$ Nm^{-2}				

2.4 at% Si delta-doping in GaAs, respectively. For the Si : B, the results are consistent with the predictions of continuum elasticity theory and with experimental work from other sources, while for the GaAs : Si the measured lattice contractions do not follow the predicted linear increase with dopant concentration and are much larger than the theory would predict. The anomalous results may be associated with the presence of defects or with the strength of Si–As bonds at the layers. It has also been shown that electrostatic attraction of the dopant ions to the free carriers is negligible for the dopant concentrations examined here.

Acknowledgements

We are grateful to Dr. R.A. Kubiak and Prof. E.H.C. Parker at Warwick University for the Si : B specimen, Dr. D.D. Perovic at the University of Toronto and Dr. Z.R. Wasilewski and Stephen Rolfe at the National Research Council of Canada for the GaAs : Si delta-doped specimen, Dr. D.D. Perovic for discussions and Dr. C.J.D. Hetherington for help with the optical moiré fringes.

References

[1] G.J. Wood, W.M. Stobbs, D.J. Smith, Phil. Mag. A 50 (1984) 375.
[2] W.M. Stobbs, G.J. Wood, D.J. Smith, Ultramicroscopy 14 (1986) 145.
[3] E.F. Schubert, Doping in III–V Semiconductors, Cambridge University Press, Cambridge, 1993.
[4] R.E. Dunin-Borkowski, Phil. Mag. A, in preparation.
[5] R. Bierwolf, M. Hohenstein, F. Phillipp, O. Brandt, G.E. Crook, K. Ploog, Ultramicroscopy 49 (1993) 273.
[6] C.J.D. Hetherington, U. Dahmen, Scanning Microscopy Supplement 6 (1992) 405.
[7] C.J.D. Hetherington, P.D. Brown, R.E. Dunin-Borkowski, Inst. Phys. Conf. Ser. 138 (1993) 255.
[8] H. Holloway, S.L. McCarthy, J. Appl. Phys. 73 (1993) 103.
[9] J.P. Suchet, Chemical Physics of Semiconductors, Van Nostrand, New York, 1965.
[10] W.B. Pearson, in: Handbook of Lattice Spacings, Structures of Metals, Pergamon Press, New York, 1967.
[11] J.F. Nye, Physical Properties of Crystals: their representation by tensors and matrices, Clarendon, Oxford, 1985.
[12] W.A. Brantley, J. Appl. Phys. 44 (1973) 534.
[13] A.R. Powell, R.A.A. Kubiak, S.M. Newstead, C. Parry, N.L. Mattey, D.W. Smith, J.C. Brighten, C.J. Emeleus, T. Naylor, E. Basaran, T.E. Whall, M.G. Dowsett, R.D. Barlow, E.H.C. Parker, J. Crystal Growth 111 (1991) 907.
[14] K. Fujii, Y. Okada, F. Orito, J. Appl. Phys. 73 (1993) 88.
[15] T. Walther, Abteilung Anorganische materialforschung, Institut für Anorganische Chemie, Universität Bonn, Römerstr, 164, D-53117 Bonn, Germany, private communication.
[16] P.F. Fewster, A.F.W. Willoughby, J. Crystal Growth 50 (1980) 648.
[17] G.P. Watson, D. Ast, A.G. Elliot, Appl. Phys. Lett. 54 (1989) 271.
[18] R.E. Dunin-Borkowski, W.O. Saxton, W.M. Stobbs, Acta Crystallogr. A 52 (1996) 705.